CNWRA ***A center of excellence in earth sciences and engineering***

A Division of Southwest Research Institute™
6220 Culebra Road • San Antonio, Texas, U.S.A. 78228-5166
(210) 522-5160 • Fax (210) 522-5155

December 7, 2001
Contract No. NRC–02–97–009
Account No. 20.01402.861

U.S. Nuclear Regulatory Commission
ATTN: Mr. Neil M. Coleman
Division of Waste Management
Two White Flint North, Mail Stop 7C 13
Washington, DC 20555

Subject: Transmittal of the deliverable "*In Situ* Permeability Measurement—Journal Paper (IM 01402.861.230)

Dear Mr. Coleman:

This letter transmits Intermediate Milestone 01402.861.230 "*In Situ* Permeability Measurement—Journal Paper." This item is identified in the fiscal year 2002 CNWRA Operations Plans. This work was largely conducted by Dr. Cynthia Dinwiddie as part of her Ph.D. thesis work. Because of the relevance of the work to ongoing studies at CNWRA, the effort has been completed as an activity under the Unsaturated and Saturated Flow Under Isothermal Conditions Key Technical Issue.

As you know, adequate characterization of the permeability of the host rocks is a topic of significance for the proposed geologic repository at Yucca Mountain. This paper presents an innovative approach to measuring permeability and explores sources of uncertainty in such measurements. The numerical models developed to evaluate the new approach enable testing of boundary conditions and assessment of the effective sample volume that is characterized by the method.

If you have any questions about this deliverable, please contact me 210.522.5540 or Dr. Cynthia Dinwiddie 210.522.6085.

Sincerely yours,

English C. Pearcy
Manager, Geohydrology and Geochemistry

cc: J. Linehan, B. Meehan, D. DeMarco, E. Whitt, J. Greeves, W. Reamer, L. Hamden, W. Ford, H. Arlt, D. Brooks, B. Leslie, W. Patrick, CNWRA Directors, CNWRA Managers, C. Dinwiddie, J. Winterle, P. Maldonado, T. Nagy (SwRI Contracts)

Washington Office • Twinbrook Metro Plaza #210
12300 Twinbrook Parkway • Rockville, Maryland 20852-1606

A new small drillhole minipermeameter probe for *in situ* permeability measurement: fluid mechanics and geometrical factors

Cynthia L. Dinwiddie

Southwest Research Institute, Center for Nuclear Waste Regulatory Analyses, San Antonio, Texas

Fred J. Molz, III

Department of Environmental Engineering & Science, Clemson University, Clemson, South Carolina.

James W. Castle

Department of Geological Sciences, Clemson University, Clemson, South Carolina

Abstract. Considerable heterogeneity is evident when permeability measurements are made on small scales, either in the field or in the laboratory on field samples. Small scale permeability measurements have commonly been made by inducing multidimensional gas flow through a sample with various configurations of the conventional surface-sealing gas minipermeameter. In order to overcome weathering and seal-quality problems, a new minipermeameter probe was designed for field application within small diameter holes drilled into an outcrop. We briefly describe the small drillhole minipermeameter, while developing in detail the associated data analysis methodology for performing *in situ* permeability measurements with this new probe. Analysis of field data, which consists of gas injection pressure and mass flow rate, is based on a numerical solution in cylindrical coordinates of the ideal gas flow equation, assuming homogeneous and isotropic conditions over the averaging volume of the measurements. In the following development, the semi-analytical inverse solution for permeability will be derived for the new small drillhole minipermeameter probe, which varies from that of the conventional surface-sealing minipermeameter probe only in the choice of the appropriate characteristic length and in the magnitude of the associated geometrical factor.

GAP Index Terms: 1) Physical Properties of Rocks: Permeability and Porosity (5114); 2) Mathematical Geophysics: Numerical Solutions (3230); 3) Hydrology: Instruments & Techniques (1894); 4) Hydrology: Unsaturated Zone (1875); 5) Exploration Geophysics: Instruments & Techniques (0994)

1. Introduction

As one of the primary engineering variables that influences contaminant recovery during remediation efforts, as well as fluid migration in general, intrinsic permeability and its three-dimensional distribution in the subsurface are candidates for the "Holy Grail" of hydrogeology. Likewise, small-scale permeability heterogeneity plays a substantial role in petroleum migration and reservoir performance, because permeability may vary over many orders of magnitude (e.g., 0.01 mD to over 10,000 mD [*Norris and Lewis*, 1991]). Permeability heterogeneities on the meter-to-micrometer scale, such as beds, laminae, internal sedimentary structures and variations in pore morphology, are the source of most retrieval difficulties during enhanced oil recovery operations, thus negatively affecting reservoir recovery efficiency [*Weber*, 1982; *Weber*, 1986; *Hurst and Rosvoll*, 1991; *Ali*, 1993; *Pickup et al.*, 1995].

Considerable heterogeneity is evident when permeability measurements are made on small scales, either in the field or on field samples in a laboratory setting. Small scale permeability measurements were traditionally made by inducing one-dimensional gas flow through a cylindrical core plug in a Hassler sleeve or cell [*Hassler*, 1944; *American Petroleum Institute*, 1960, 1998]. Recently, such measurements have also commonly

been made by inducing multidimensional gas flow through a sample with various configurations of the conventional surface-sealing gas minipermeameter (also known in the literature as a probe permeameter).

In the petroleum industry, cylindrical plugs have traditionally been extracted from continuous core at 0.30-meter intervals for Hassler-sleeve permeability measurement [*Clelland*, 1984, *Dubrule and Haldorsen*, 1986; *Goggin et al.*, 1988; *Robertson and McPhee*, 1990; *Corbett and Jensen*, 1992*a*, *b*], which preserves a majority of the core while minimizing associated costs. Except for relatively homogeneous formations, this scale of permeability measurement is in an ill-defined geologic region, falling within the range of laminae and lamina sets [*Allen*, 1988; *Hurst and Rosvoll*, 1991; *Jensen et al.*, 1994; *Hurst et al.*, 1995]. Furthermore, core plug samples tend to be biased toward the more consolidated, less permeable and less friable sections [*Robertson and McPhee*, 1990; *Hurst*, 1993; *Zheng et al.*, 2000]. As an example, the effect of this arbitrary sampling density on Hassler-sleeve measurements for the case of tight gas sands is that magnitudes of permeability less than 100 mD frequently result, even when coarser-grained beds that would operate as preferential flow channels or "thief zones" are clearly present. At present, the scale of sedimentary heterogeneity is best resolved by use of the minipermeameter, which allows investigation of permeability heterogeneity at much greater (and statistically significant) sampling densities and on much smaller scales than is possible with the traditional technique [*Jensen*, 1990; *Robertson and McPhee*, 1990; *Hurst and Rosvoll*, 1991; *Corbett and Jensen*, 1992*a*; *Bourke*, 1993; *Halvorsen*, 1993; *Kara et al.*, 1993; *Hurst and Goggin*, 1995; *Tidwell and Wilson*, 1997].

The literature documents use of the conventional surface-sealing minipermeameter probe for measurements made on outcrop surfaces, core plugs, slabbed cores, or on large cut blocks. One motivation for using cores, plugs or blocks of rock is that natural weathering processes may greatly affect permeability values obtained from exposed outcrop surfaces. The weathering effect has been shown to extend up to several inches below the rock surface [*C.B. Forster et al.*, 3-D fluid flow simulation in a clastic reservoir analog: based on integrated 3-D GPR and outcrop data from the Ferron Sandstone at Coyote Basin, Utah, submitted to *The Fluvial-Deltaic Ferron Sandstone: Regional to Wellbore Scale Outcrop Analog Studies and Reservoir Modeling*, edited by T.C. Chidsey, Jr., R.D. Adams, and T.H. Morris, *AAPG Memoir*, 2001]. The authors' interest in this subject matter was spurred by involvement in U.S. Department of Energy oil reservoir architecture research through the Office of Fossil Energy [*Castle et al.*, 2000]. Permeability data were sought from outcrop analogues (shallow-marine Upper Cretaceous Straight Cliffs Formation near Escalante, Utah), but being cognizant of the need to avoid measurements obtained from weathered surfaces, a core drill was selected to retrieve cylindrical plugs, from which permeability data could be collected in a laboratory environment from the distal (and less weathered) end of the plug. Because the selected sandstone outcrops were weakly cemented and friable, the core drill frequently produced pulverized sand or significantly disturbed plugs. It became apparent that obtaining sandstone samples for use in the lab was not always feasible, and certainly was not in this case.

Beyond the issue of weathering, there are other rationales for discouraging use of the conventional minipermeameter probe in a field setting. When applying it to natural rock outcroppings in the field, as opposed to cut specimens in an automated laboratory setting, seal-quality problems are often encountered due to irregular, rough surfaces, and difficulties associated with manually holding the probe stationary while applying a uniform normal force of the optimal magnitude on the tip seal.

To overcome weathering and seal-quality problems, a new minipermeameter probe has been developed, designed in particular for application inside a small drillhole [*Dinwiddie*, 2001]. In the process of setting up the authors' original field site for plug recovery, it was discovered that it is a simple task to drill small, high quality holes in the outcrop with a masonry drill. The creation of the hole is followed by probe insertion, seal expansion and *in situ* calculation of permeability via measurement of the injection pressure, flow rate, and knowledge of the system's flow geometry, as characterized by geometric factors to be presented herein. Advantages of this *in situ* approach are (1) minimization of the influence of weathering on permeability; (2) elimination of the need to correct lab samples for lack of overburden [*Dubrule and Haldorsen*, 1986; *Jones*, 1992; *Gibbons et al.*, 1993; *Hurst et al.*, 1995; *American Petroleum Institute*, 1998; *Zheng et al.*, 2000]; (3) provision of a superior sealing mechanism around the air injection zone (with which it is a simple matter to consistently apply the necessary force for a seal, while maintaining a geometrical factor that is independent of the operator); and (4) the potential for measurement collection at multiple depths below the outcrop surface. In this article we will briefly describe the small drillhole minipermeameter probe (the interested reader is referred to a future publication [*C.L. Dinwiddie et al.*, The new small drillhole minipermeameter probe: design,

operation, and performance characteristics, manuscript in preparation, 2002] for an in-depth description of the probe and its design), while developing in detail the associated data analysis methodology for performing *in situ* permeability measurements inside small diameter holes. Analysis of field or laboratory data, which consists of gas injection pressure and mass flow rate, is based on the numerical solution in cylindrical coordinates of the ideal gas flow equation, assuming homogeneous and isotropic conditions over the averaging volume of the measurements. The overall analytical approach follows that developed by *Goggin* [1988], while excluding corrections for gas slippage and high velocity flow effects (the methods of correction for these phenomena were developed and fully described in *Goggin et al.* [1988], and are unchanged for the new probe geometry).

2. Small Drillhole Minipermeameter Probe Dimensions

The new small drillhole minipermeameter probe is designed for application in cylindrical holes drilled with a standard $^5/_8$-in (1.59-cm) masonry drill bit. This drill bit readily cut a 1.8-cm diameter hole in the shallow marine sandstone at the Escalante, Utah field site. The diameter of the hole resulting from this particular drill bit may vary slightly from one rock type to another. The probe was designed for use in holes with a maximum depth of 10 cm; however, 1.59-cm diameter masonry drill bits with a length of at least 30 cm are readily available, and modification of the current probe design for application in deeper holes would be an easy task. Thus, deeper holes could be drilled, enabling permeability measurement at multiple depths below the outcrop surface, and allowing collection of a three-dimensional data set.

Like the tip-seal of the surface-sealing minipermeameter probe, the rubber seal of the drillhole probe is a cylindrical annulus, but in this case axial compression causes the seal to expand like a packer against the sides of the drill hole. The seal, which is composed of smooth-finish pure gum rubber tubing with a $^3/_{16}$-in (4.76-mm) inner diameter, $^9/_{16}$-in (14.29-mm) outer diameter, and $^3/_{16}$-in (4.76-mm) wall thickness, is used to secure the probe at the distal end of the drill hole, while isolating the injection zone from the ejection zone.

3. Theoretical Analysis—Semi-Analytical Inverse Solution

Through the first numerical models of the conventional surface-sealing minipermeameter flow system, *Goggin et al.* [1988] demonstrated that the inverse solution for probe permeability replaces the one-dimensional Hassler-sleeve geometric combination L/A (where L is the length of a cylindrical core plug and A is its cross-sectional area) with the dimensionally compatible term $1/(aG_o)$, where the inlet radius, a, was selected as the characteristic length, and G_o is a dimensionless geometrical factor [*Robertson and McPhee*, 1990; *Sutherland et al.*, 1993]. Thus, the semi-analytical inverse solution for permeability, k_g (D; 1 D = 0.986923×10^{-12} m^2), when measured by the conventional surface-sealing minipermeameter is:

$$k_g = \frac{2\mu_g q_1 P_1}{aG_o\left(P_1^2 - P_0^2\right)}, \tag{1}$$

where μ_g = gas viscosity (cp; 1 cp = 1×10^{-3} N s m^{-2}), q_1 = volumetric flow rate at injection pressure (cm^3 s^{-1}; 1 cm^3 s^{-1} = 1×10^{-6} m^3 s^{-1}), P_1 = injection pressure, and P_0 = atmospheric pressure (atm; 1 atm = 101 325 N m^{-2}). The geometrical factor, when calculated numerically for a given sample and probe geometry, accounts for the complex multidimensional flow pattern throughout the porous medium, capturing the edge effects associated with the geometry of the sample and probe, and thus boundary conditions that are simply not accounted for by an empirical calibration using core plugs. This can be particularly true when using a calibration relationship [*Robertson and McPhee*, 1990; *Sutherland et al.*, 1993] to solve for permeability on a sample with a strongly differing geometry or size than that of the core plugs used in the calibration exercise.

The validity of the minipermeameter inverse solution presented in Equation (1) has been definitively established under Darcy flow conditions through many correlative studies with Hassler-sleeve measurements [*Goggin et al.*, 1988; *Halvorsen and Hurst*, 1990; *Robertson and McPhee*, 1990; *Corbett and Jensen*, 1992*a*; *Jensen and Corbett*, 1992; *Jones*, 1992; *Ali*, 1993; *Goggin*, 1993; *Sharp et al.*, 1994; *Garrison et al.*, 1996]. As

a result of the confidence gained in the solution by *Goggin et al.* [1988] throughout the last decade, tedious equipment-specific empirical calibrations with Hassler-sleeve measurements are no longer required for every new tip seal geometry or every new injection pressure prior to conducting an investigation [*Young*, 1989; *Garrison et al.*, 1996].

In the following development, the semi-analytical inverse solution for permeability will be derived for the new small drillhole minipermeameter probe, which varies from Equation (1) only in the choice of the appropriate characteristic length and in the magnitude of the associated geometrical factor.

3.1. Minipermeameter measurements made in a small drill hole

As first described by *Dinwiddie et al.* [1999] and illustrated below in Figure 1, an annular rubber tip seal undergoes axial compression, causing the seal to expand like a packer against the drill hole. It is used to seal the probe in the bottom of the drill hole, while isolating the injection zone from the ejection zone. Pressure within the sealed-off region is maintained above that of the atmosphere, so that gas enters the porous medium, flows around the tip seal, and exits to the rock surface either in the drill hole or at the cliff face (both are at atmospheric pressure). Because the small drillhole minipermeameter probe is intended for use as a field instrument, the infinite half-space flow system solution is of particular interest. This will be approximated numerically with a finite-difference algorithm for a semi-infinite domain with no flow across distant boundaries.

3.2. The steady-state mass conservation equation for radially symmetric compressible ideal gas flow

The geometry of the drillhole probe compels the use of a cylindrical coordinate system. In this case, mass flux is given by:

$$\rho_g \vec{u}_g = \rho_g u_{rg} \vec{i} + \rho_g u_{zg} \vec{j}, \tag{2}$$

where ρ_g is gas density, $\vec{u}_g$ is the darcy flux, and r and z are radial and vertical coordinate directions, respectively. Thus, the steady-state mass conservation equation governing radially symmetric gas flow in a porous medium has the following representation:

$$\frac{1}{r}\frac{\partial}{\partial r}\left(r\rho_g u_{rg}\right) + \frac{\partial}{\partial z}\left(\rho_g u_{zg}\right) = 0. \tag{3}$$

Given the following assumptions: 1) darcy flow (no high velocity flow or inertial effect, and no gas slippage or Klinkenburg effect); 2) ideal gas compressibility (the average gas compressibility factor, $\bar{z}$, is approximately unity for ambient conditions); and 3) homogeneous and isotropic permeability (k_g is constant) within the measurement's averaging volume, the expression for mass flux is:

$$\rho_g u_{\varphi g}\Big|_{\varphi=r,z} = -\frac{k_g}{\mu_g}\left(\frac{M_{wt} P_g}{RT}\right)\frac{\partial P_g}{\partial \varphi}, \tag{4}$$

where M_{wt} is the molecular weight of the gas, P_g is the gas pressure, R is a gas constant, T is temperature, and φ is a dummy coordinate direction representing either r or z.

To linearize Equation (4), one may define an ideal gas pseudo-potential, Φ, in order to take advantage of the Kirchoff transform. Following *Goggin et al.* [1988] in general, and *Aronson* [1999] in particular:

$$\Phi \equiv \frac{M_{wt}}{\mu_g RT}\frac{P_g^2}{2}. \tag{5}$$

Whereas gas viscosity is a weak function of pressure, it varies strongly with temperature and water vapor content. Thus, for approximately isothermal conditions, the relationship defined in Equation (5) results in a satisfactory linearization of the governing equation under ambient conditions. The components of the pseudo-potential gradient are:

$$\left.\frac{\partial \Phi}{\partial \varphi}\right|_{\varphi=r,z} = \frac{M_{wt}P_g}{\mu_g RT}\frac{\partial P_g}{\partial \varphi}. \tag{6}$$

Therefore, Equation (4) can be written as:

$$\rho_g u_{\varphi g}\big|_{\varphi=r,z} = -k_g \frac{\partial \Phi}{\partial \varphi}. \tag{7}$$

Substitution of Equation (7) into the steady-state conservation equation [i.e. Equation (3)] yields:

$$\frac{1}{r}\frac{\partial}{\partial r}\left(rk_g\frac{\partial \Phi}{\partial r}\right)+\frac{\partial}{\partial z}\left(k_g\frac{\partial \Phi}{\partial z}\right)=0. \tag{8}$$

Recalling that k_g is assumed homogeneous and isotropic over the averaging volume of the measurement (i.e., a constant), we obtain the general steady-state gas flow equation in cylindrical coordinates:

$$\frac{\partial^2 \Phi}{\partial r^2}+\frac{1}{r}\frac{\partial \Phi}{\partial r}+\frac{\partial^2 \Phi}{\partial z^2} = 0. \tag{9}$$

3.3. Boundary Conditions of the Small Drillhole Minipermeameter Probe System

The boundary conditions governing the pressure distribution, and hence the mass flux field, are defined by a semi-infinite domain that makes use of symmetry, has no flow across distant boundaries, no flow across the

seal, a constant injection pressure, and atmospheric pressure at both the outcrop and adjacent drillhole surface. Specifically, the boundary conditions for the geometry shown in Figure 2 are as follows:

$$
\begin{aligned}
P_{inlet} &= P_1 \quad \text{for} \quad 0 \le r \le B \quad \text{at } z = -\left(\frac{W-D}{B}\right) r + W \\
&\qquad\quad \text{for} \quad H \le z \le D \quad \text{at } r = B \\
P_{outlet} &= P_0 \quad \text{for} \quad 0 \le z \le L \quad \text{at } r = B \\
&\qquad\quad \text{for} \quad B \le r \le R_{max} \quad \text{at } z = 0 \\
\left.\frac{\partial P_g}{\partial r}\right|_{r=B} &= 0 \quad \text{for} \quad L \le z \le H \quad \text{at } r = B \\
\left.\frac{\partial P_g}{\partial r}\right|_{r=R_{max}} &= 0 \quad \text{for} \quad 0 \le z \le Z_{max} \quad \text{at } r = R_{max} \\
\left.\frac{\partial P_g}{\partial z}\right|_{z=Z_{max}} &= 0 \quad \text{for} \quad 0 \le r \le R_{max} \quad \text{at } z = Z_{max} \\
\left.\frac{\partial P_g}{\partial r}\right|_{r \to 0} &= 0 \quad \text{for} \quad W \le z \le Z_{max} \quad \text{as } r \to 0.
\end{aligned}
\tag{10}
$$

Following the procedure developed by *Goggin et al.* [1988], Equation (9) and the boundary conditions given in Equation (10) are expressed in dimensionless units by dividing each dimension by the characteristic length, B, such that any given dimension φ can be written in terms of the dimensionless variable φ_D:

$$\varphi = B\varphi_D . \tag{11}$$

Recollecting the need to recast pressure in terms of pseudo-potential for the purpose of linearization, we define the following dimensionless constants and variables (choosing the characteristic length to be the drillhole radius, B, and calling Φ_1 and Φ_0 the injection and atmospheric pseudo-potential, respectively):

$$
\begin{gathered}
z_D = \frac{z}{B};\ r_D = \frac{r}{B};\ \Phi_D = \frac{\Phi - \Phi_0}{\Phi_1 - \Phi_0}; \\
L_D = \frac{L}{B};\ H_D = \frac{H}{B};\ D_D = \frac{D}{B};\ W_D = \frac{W}{B};\ Z_{D_{max}} = \frac{Z_{max}}{B};\ R_{D_{max}} = \frac{R_{max}}{B}.
\end{gathered}
\tag{12}
$$

Substituting these definitions into Equation (9), yields:

$$\frac{\partial^2 \Phi_D}{\partial r_D^2} + \frac{1}{r_D}\frac{\partial \Phi_D}{\partial r_D} + \frac{\partial^2 \Phi_D}{\partial z_D^2} = 0. \tag{13}$$

While it may be possible to solve Equation (13) analytically, subject to the following boundary conditions, herein it is solved numerically through finite-difference approximation. As developed by *Dinwiddie* [2001], the

dimensionless boundary conditions governing the pseudo-potential distribution, and hence the mass flux field for the half-space geometry, are given by:

$$\Phi_D(\Phi_1)=1 \qquad \text{for} \quad 0<r_D\le 1 \qquad \text{at} \quad z_D=-(W_D-D_D)r_D+W_D$$
$$\text{for} \quad H_D\le z_D\le D_D \qquad \text{at} \quad r_D=1$$

$$\Phi_D(\Phi_0)=0 \qquad \text{for} \quad 0\le z_D\le L_D \qquad \text{at} \quad r_D=1$$
$$\text{for} \quad 1\le r_D\le R_{D_{max}} \qquad \text{at} \quad z_D=0$$

$$\left.\frac{\partial\Phi_D}{\partial r_D}\right|_{r_D=1}=0 \quad \text{for} \quad L_D\le z_D\le H_D \quad \text{at} \quad r_D=1 \tag{14}$$
$$\left.\frac{\partial\Phi_D}{\partial r_D}\right|_{r_D=R_{D_{max}}}=0 \quad \text{for} \quad 0\le z_D\le Z_{D_{max}} \quad \text{at} \quad r_D=R_{D_{max}}$$
$$\left.\frac{\partial\Phi_D}{\partial z_D}\right|_{z_D=Z_{D_{max}}}=0 \quad \text{for} \quad 0<r_D\le R_{D_{max}} \quad \text{at} \quad z_D=Z_{D_{max}}$$
$$\left.\frac{\partial\Phi_D}{\partial r_D}\right|_{r_D\to 0}=0 \quad \text{for} \quad W_D\le z_D\le Z_{D_{max}} \quad \text{as} \quad r_D\to 0$$

3.4. Geometrical Factors, the Integral Form of Darcy's Law, and the Small Drillhole Minipermeameter Inverse Solution for Permeability

The mass injection rate, $\dot{m}_{o_1}$, entering through the cylindrical surface between H and D (Figure 2), is given theoretically by the following expression:

$$\dot{m}_{o_1}=\int_0^{2\pi}\int_H^D\left(\rho_g u_{gr}\big|_{r=B}\right)B\,dz\,d\theta. \tag{15}$$

The mass injection rate, $\dot{m}_{o_2}$, entering the conical surface at the distal end of the drill hole is given by the following line integral along the path $z=-\left(\frac{W-D}{B}\right)r+W$:

$$\dot{m}_{o_2}=\int_0^{2\pi}\int_{r\to 0,D}^{B,W}\rho_g\vec{u}_g\cdot d\vec{L}\,r\,d\theta=\int_0^{2\pi}\int_{r\to 0}^{B}\rho_g u_{gr}\,dr\,r\,d\theta+\int_0^{2\pi}\int_D^W\rho_g u_{gz}\,dz\,r\,d\theta, \tag{16}$$

where $\rho_g\vec{u}_g=\rho_g u_{gr}\hat{i}+\rho_g u_{gz}\hat{j}$ and $d\vec{L}=dr\,\hat{i}+dz\,\hat{j}$. The first integral on the RHS represents the *horizontal* component of the gas mass injection rate through the conical surface inlet, and the second integral

on the RHS represents the *vertical* component of the gas mass injection rate through the conical surface inlet. Thus, the total rate of mass injection into the system $\left(\dot{m}_o = \dot{m}_{o_1} + \dot{m}_{o_2}\right)$ is then given by:

$$\begin{aligned}\dot{m}_o = &\int_0^{2\pi}\int_H^D \left(\rho_g u_{gr}\Big|_{r=B}\right) B\,dz\,d\theta \quad + \\ &\int_0^{2\pi}\int_{r\to 0}^{B} \left(\rho_g u_{gz}\Big|_{z=-\left(\frac{W-D}{B}\right)r+W}\right) r\,dr\,d\theta \quad + \\ &\int_0^{2\pi}\int_D^W \left(\rho_g u_{gr}\Big|_{r=-\left(\frac{B}{W-D}\right)z+\frac{WB}{W-D}}\right) r\,dz\,d\theta.\end{aligned} \tag{17}$$

For axi-symmetric flow, and utilizing Equation (7), the total rate of mass injection is simplified to:

$$\begin{aligned}\dot{m}_o = &\,2\pi B\int_H^D \left\{-k_g\frac{\partial\Phi}{\partial r}\right\}_{r=B} dz \quad + \\ &2\pi\int_{r\to 0}^{B} \left\{-k_g\frac{\partial\Phi}{\partial z}\right\}_{z=-\left(\frac{W-D}{B}\right)r+W} r\,dr \quad + \\ &2\pi\int_D^W \left\{-k_g\frac{\partial\Phi}{\partial r}\right\}_{r=-\left(\frac{B}{W-D}\right)z+\frac{WB}{W-D}} r\,dz.\end{aligned} \tag{18}$$

Recall from the definitions in Equations (12) that the dimensionless pseudo-potential is determined in the following manner:

$$\Phi_D = \frac{\Phi - \Phi_0}{\Phi_1 - \Phi_0}, \tag{19}$$

so, the derivative of Φ_D taken with respect to Φ is given by:

$$\frac{d\Phi_D}{d\Phi} = \frac{1}{\Phi_1 - \Phi_0}. \tag{20}$$

Also, from Equation (5), we have the following relationship:

$$\Delta\Phi = \left(\Phi_1 - \Phi_0\right) = \frac{M_{wt}}{\mu_g RT}\left[\frac{P_1^2 - P_0^2}{2}\right]. \tag{21}$$

Now, since any dimensionless variable is given by $\varphi_D\big|_{\varphi=r,z} = \varphi / B$, it is also true that $d\varphi_D = d\varphi / B$, *and* $\varphi d\varphi = B^2 \varphi_D d\varphi_D$. Then, by the Chain Rule and Equations (20) and (21), we have:

$$\left.\frac{\partial \Phi}{\partial \varphi}\right|_{\varphi=r,z} = \frac{\partial \Phi}{\partial \Phi_D}\frac{\partial \Phi_D}{\partial \varphi_D}\frac{\partial \varphi_D}{\partial \varphi} = \frac{(\Phi_1 - \Phi_0)}{B}\frac{\partial \Phi_D}{\partial \varphi_D} = \frac{M_{wt}}{\mu_g RT}\left[\frac{P_1^2 - P_0^2}{2B}\right]\frac{\partial \Phi_D}{\partial \varphi_D}. \tag{22}$$

Thus, the dimensionless form of Equation (18) is as follows:

$$\begin{aligned} \dot{m}_o = &-2\pi B \int_{H_D}^{D_D} k_g \frac{M_{wt}}{\mu_g RT}\left[\frac{P_1^2 - P_0^2}{2}\right]\left.\frac{\partial \Phi_D}{\partial r_D}\right|_{r_D=1} dz_D \\ &-2\pi B \int_{r_D \to 0}^{1} k_g \frac{M_{wt}}{\mu_g RT}\left[\frac{P_1^2 - P_0^2}{2}\right]\left.\frac{\partial \Phi_D}{\partial z_D}\right|_{z_D=-(W_D-D_D)r_D+W_D} r_D dr_D \\ &-2\pi B \int_{D_D}^{W_D} k_g \frac{M_{wt}}{\mu_g RT}\left[\frac{P_1^2 - P_0^2}{2}\right]\left.\frac{\partial \Phi_D}{\partial r_D}\right|_{r_D=-\left(\frac{1}{W_D-D_D}\right)z_D+\frac{W_D}{W_D-D_D}} r_D dz_D. \end{aligned} \tag{23}$$

Utilizing $\Delta\Phi$, as defined in Equation (21), Equation (23) for the total rate of mass injection simplifies to:

$$\begin{aligned} \dot{m}_o = &-2\pi B k_g \Delta\Phi \int_{H_D}^{D_D} \left.\frac{\partial \Phi_D}{\partial r_D}\right|_{r_D=1} dz_D \\ &-2\pi B k_g \Delta\Phi \int_{r_D \to 0}^{1} \left.\frac{\partial \Phi_D}{\partial z_D}\right|_{z_D=-(W_D-D_D)r_D+W_D} r_D dr_D \\ &-2\pi B k_g \Delta\Phi \int_{D_D}^{W_D} \left.\frac{\partial \Phi_D}{\partial r_D}\right|_{r_D=-\left(\frac{1}{W_D-D_D}\right)z_D+\frac{W_D}{W_D-D_D}} r_D dz_D. \end{aligned} \tag{24}$$

The geometrical factor, G_o, is a function of all system boundary conditions (i.e. dependent on both probe *and* sample geometry) and is defined as follows:

$$G_o = 2\pi \int_{H_D}^{D_D} \left.\frac{\partial \Phi_D}{\partial r_D}\right|_{r_D=1} dz_D + 2\pi \int_{r_D \to 0}^{1} \left.\frac{\partial \Phi_D}{\partial z_D}\right|_{z_D=-(W_D-D_D)r_D+W_D} r_D dr_D + 2\pi \int_{D_D}^{W_D} \left.\frac{\partial \Phi_D}{\partial r_D}\right|_{r_D=-\left(\frac{1}{W_D-D_D}\right)z_D+\frac{W_D}{W_D-D_D}} r_D dz_D . \quad (25)$$

Finally, Equation (24) reduces to the following integral form of Darcy's law as determined from the rate of mass injection:

$$\dot{m}_o = -BG_o k_g \Delta\Phi . \quad (26)$$

Equation (26) is superficially very similar to Equation (1) of *Goggin et al.* [1988], which is commonly referred to in the literature as a "modified form of Darcy's law". However, whereas the *Goggin et al.* [1988] equation applies to the geometry of a conventional surface-sealing minipermeameter probe, Equation (26) applies specifically to the drillhole probe system geometry through the geometrical combination BG_o. Using the ideal gas law, the total rate of mass injection may be expressed as:

$$\dot{m}_o = -BG_o k_g \frac{\rho}{\mu_g P_1}\left[\frac{P_1^2 - P_0^2}{2}\right], \quad (27)$$

and solving for permeability yields:

$$k_g = -\frac{\dot{m}_0}{\rho}\frac{\mu_g P_1}{BG_o\left[\frac{P_1^2 - P_0^2}{2}\right]} = \frac{2\mu_g q_1 P_1}{BG_o\left[P_1^2 - P_0^2\right]}. \quad (28)$$

4. Finite-Difference Numerical Models for Determination of Geometrical Factor Curves

4.1. Node System, Difference Equation, and the Computational Molecule

Two-dimensional axi-symmetric compressible gas flow from the injection zone to the atmospherically-exposed rock surface was numerically simulated by a mesh-centered finite-difference Fortran algorithm. The flow domain mesh features variable discretization in both coordinate directions, which becomes increasingly fine as the critical tip seal region is approached such that the rapidly increasing pseudo-potential gradient is accurately represented in this vicinity. The mesh system in cylindrical coordinates (r_D, z_D) for the geometry of the probe used in laboratory and field testing is illustrated in Figure 3. The conical boundary nodes, which simulate the tapered end of the drill hole, have equal spacings in both the r_D and z_D directions, and fall precisely on the $z_D = -(W_D - D_D)r_D + W_D$ line.

Truncated Taylor series expansions (i.e., standard second-order formulations with truncation error of order $O(\Delta\varphi_D^2)$) were used to algebraically approximate the derivatives of Equation (13) in order to solve the differential equation for $\Phi_D(r_D, z_D)$ throughout the system domain. Given the boundary conditions of Equation (14) and initialization of the unknown pseudo-potentials in the interior of the flow domain to some reasonable value, the algebraic difference equation is rearranged into a 5-point computational molecule that sweeps iteratively through the node system, continuously updating $\Phi_{D_{i,j}}$ in terms of its nearest neighbors ($\Phi_{D_{i-1,j}}, \Phi_{D_{i+1,j}}, \Phi_{D_{i,j-1}}, \Phi_{D_{i,j+1}}$), while overcorrecting at each iteration with a successive-over-relaxation factor, ω, equal to 1.4 to speed convergence. No flow boundaries are handled in the usual way with fictitious image nodes.

The far-field boundaries (R_{Dmax} and Z_{Dmax}) of the numerical models were selected through an iterative procedure. For example, the geometrical factor for the geometry of the laboratory and field-tested probe (Figure 2) was repeatedly determined numerically for increasingly distant far-field boundaries (see *Chen* [1992]). As the distance to these boundaries increased, the geometrical factor increased at a decreasing rate until edge effects were no longer significant (Figure 4).

4.2. Calculation of Mass Balance Error

The pseudo-potential gradients were computed at each boundary node with a rearrangement of the Taylor series expansion for the second derivative in order to calculate the mass balance error. The rate of mass entering or exiting each boundary per unit width is obtained through numerical integration of the dimensionless boundary node pseudo-potential gradients in a manner similar to that of Simpson's Rule, where a second-degree polynomial is fit through the dimensionless pseudo-potential gradient at each of three neighboring nodes, such that a running sum may be computed. However, this method is somewhat more complicated than that of Simpson's Rule due to the variable node spacing. In cases where the number of nodes along a given boundary is not even, the Trapezoidal Rule is utilized to sum the mass passing between the last two nodes. Whenever use of the Trapezoidal Rule is required, it is employed where the flux is at a minimum such that the numerical accuracy is maximized.

The total rate of mass entering the system per unit length was calculated by summing up the individual contributions at the two injection surfaces (the vertical surface between H_D and D_D at $r_D = 1$, and the conical surface created by the shape of the drill bit), plus the virtually negligible positive contributions along the left-most boundary as $r_D \rightarrow 0$ between W_D and Z_{Dmax}, and the uppermost boundary at $z_D = Z_{Dmax}$ between $r_D \rightarrow 0$ and R_{Dmax}. The total rate of mass exiting the system per unit length was calculated by summing up the individual contributions at the two ejection surfaces (the vertical surface between $z_D = 0$ and L_D at $r_D = 1$, and the boundary at the outcrop surface between $r_D = 1$ and R_{Dmax} at $z_D = 0$), plus the virtually negligible contribution along the right-most boundary at $r_D = R_{Dmax}$ between $z_D = 0$ and Z_{Dmax}. The mass balance error was then calculated by subtracting from unity the ratio of the total rate of mass entering the system per unit length to the total rate of mass exiting the system per unit length. Mass balance errors associated with the following simulations ranged from 2.2% to 4.2%.

4.3. Numerical Solutions to the Small Drillhole Minipermeameter Probe System with Geometry Variation

The baseline numerical solution (Figure 5) is for the small drillhole minipermeameter probe/sample geometry that was tested both in the laboratory and field, i.e., the system dimensions of Figure 2 and the numerical mesh of Figure 3. Numerical solutions were then determined for a variety of small drillhole minipermeameter probe and sample geometries, including drill holes of varying depth, varying seal lengths, and situations where the probe is inserted only part-way into the drill hole, producing an increased head-space and injection area. Rather than illustrating the numerical solution to each of these situations, one representative solution will be shown for each, and the effect of these variations on the geometrical factors will be illustrated through geometrical factor curves in a manner similar to that of *Goggin et al.* [1988].

4.3.1. The Geometrical Factor as a Function of Drillhole Depth. Numerical solutions were determined for the small drillhole minipermeameter probe inside holes of varying depth. Given that the dimensionless expanded seal length and headspace remain equivalent to those of the baseline scenario, we illustrate the numerical solution (Figure 6) for the innermost data point on this particular geometric factor curve: i.e. the solution for the probe in a drill hole of the shallowest possible depth. With increasing dimensionless drillhole depth, W_D, the geometrical factor decreases and slowly approaches an asymptotic value (Figure 7). This is to be expected as one considers the inverse solution given by Equation (28). For a homogeneous averaging volume (constant k_g), a constant drillhole radius, B, constant ambient conditions (μ_g and P_0), and a constant injection pressure, P_I, the only variables with changing geometry are the flow rate, q_I, and the geometrical factor, G_o. For the smallest drillhole depths, the porous medium provides little resistance to flow because the seal is in close proximity to the outcrop surface and a relatively large flow rate would be expected. Thus, the geometrical factor is also relatively large in order to balance this geometrical effect. As the drillhole depth increases, the average distance through which gas must flow also increases, lengthening streamlines, increasing the measurement averaging volume, and contributing to a greater overall resistance to flow for the same injection pressure. A corresponding decrease in the flowrate is the result, along with a proportional decrease in the geometrical factor [see also *Goggin et al.*, 1988].

4.3.2. The Geometrical Factor as a Function of Seal Length. Numerical solutions were determined for the small drillhole minipermeameter probe with seals of varying length. Given that the dimensionless drillhole depth and vertical headspace remain equivalent to those of the baseline scenario, we illustrate the numerical solution (Figure 8) for the outermost data point on this particular geometrical factor curve: i.e. the solution for a probe equipped with the longest possible seal. With increasing dimensionless seal length, $a_D = H_D - L_D$, the geometrical factor decreases and slowly approaches an asymptotic value (Figure 9). The dimensionless seal length and the dimensionless distance to the seal, L_D, are directly related to each other when the dimensionless drillhole depth and vertical headspace are held constant. Again, for a homogeneous averaging volume, constant drillhole radius, constant ambient conditions, and constant injection pressure, the flow rate and the geometrical factor are the only variables that change as a function of probe/sample geometry. Short seals provide much less resistance to flow than longer seals, so with the same reasoning as before, a short seal infers a high flow rate, which must be balanced by a large geometrical factor. Long seals increase the distance through which gas must flow in the porous material before exiting to the atmosphere, providing increased flow resistance, lower flow rates, and smaller geometrical factors.

4.3.3. The Geometrical Factor as a Function of Headspace. Numerical solutions were determined for the small drillhole minipermeameter probe with varying vertical head-space, or available injection area. Given that the dimensionless drillhole depth, drillhole radius, and seal length remain equivalent to those of the baseline scenario, we illustrate the numerical solution (Figure 10) for the probe in a drill hole with maximum vertical headspace (proximal edge of seal located at outcrop surface). The geometrical factor exhibits linear dependence on the dimensionless vertical headspace or injection area, given here as the position of the distal end of the seal, H_D, when the dimensionless drillhole depth, W_D, and seal length, $a_D = H_D - L_D$, are held constant (Figure 11). Likewise, it has been shown (Figure 12) that for a flattened drillhole (no conical drill bit impression at the distal end of the hole), the geometrical factor is again a linear function of the drill hole radius. In each case, the greater the headspace, whether in vertical or radial extent, the greater the geometrical factor, because the larger the injection surface, the greater the volumetric flow rate (all other parameters being equal).

5. Discussion and Future Work

Knowledge gained from the geometrical factor curves may be used to design, build and test future versions of the small drillhole minipermeameter probe. In a manner following *Suboor and Heller* [1995], system dimensions (e.g., seal length) may be selected based on the regions of geometrical factor curves that exhibit greater stability. For example, the dimensionless geometrical factor applicable to the probe and system geometry used during laboratory and field-testing was 9.49, and as a function of seal length this geometrical factor falls in a rapidly increasing region of the geometrical factor curve (Figure 9). On the other hand, the design of the field probe yields a geometrical factor that is in a very stable region of the curve that is a function

of drillhole depth (Figure 7). Thus, the end-user's confidence in the magnitude of the geometrical factor to be used in the calculation of permeability [Equation (28)] is augmented when the seal is relatively long and the drillhole depth is relatively deep, despite possible slight deviations from the assumed system geometry. As a counterbalance to this confidence, a decrease in resolution will result when employing longer seals, so careful analysis of both the field objective and the expected scale of heterogeneity must be undertaken prior to settling on a probe design.

The geometrical factor is a function of the geometry and boundary conditions of both the probe and the sample volume, resulting in an obvious trend: smaller sample averaging volumes result in larger geometrical factors. Again, this can be understood within the context of the weak resistance to flow that a small sample presents. With little resistance, the flow rate will be large for a given injection pressure, as will the geometrical factor if the computed permeability is to remain unchanged. Finally, it should be apparent that the only condition under which the geometrical factor is purely a function of the probe's dimensions is when the interrogated sample volume is large in comparison to the size of the probe. The interested reader is referred to a future publication [*F.J. Molz et al.*, A physical basis for calculating spatial weighting functions of instruments in homogeneous systems, submitted to *Water Resources Research*, 2000] for an in-depth study of the averaging volume of minipermeameter measurements.

An investigation of the extent of weathering phenomena could commence as a result of exploiting the unique geometry of the small drillhole minipermeameter probe. Geometrical factors are known (Figure 7) for the current design of the field probe for the minimum penetration depth (Figure 6) up to a depth of about 10 cm (Figure 5). Potentially, a very interesting study could be conducted focusing on the distributions of permeability values collected at incrementally increasing depths into various rock outcrops.

6. Conclusions

The new small drillhole minipermeameter probe is especially suited for use in a field setting. Field-testing in consolidated sandstone has indicated that this probe configuration works better in the field than the conventional surface-sealing minipermeameter probe, because drilling produces a smooth and non-weathered surface, and the normal force applied by the seal to the walls of the drill hole is more easily controlled by a mechanical torque wheel than by hand-held methods.

In this article the small drillhole minipermeameter probe was briefly described, while the associated data analysis methodology for performing *in situ* permeability measurements was developed in detail. The semi-analytical inverse solution for permeability was derived for the drillhole probe, which varies from that of the conventional surface-sealing minipermeameter probe only in the choice of the appropriate characteristic length and in the magnitude of the associated geometrical factor. Analysis of field data, which consists of gas injection pressure and mass flow rate, is based on the numerical solution in cylindrical coordinates of the ideal gas flow equation, assuming homogeneous and isotropic conditions over the averaging volume of the measurements. Numerical modeling results are presented in an effort to examine the effects of probe and sample geometry on the magnitude of the geometrical factor. Two-dimensional axi-symmetric compressible gas flow from the injection zone of a drillhole probe to the atmospherically-exposed rock surface was numerically simulated by a mesh-centered finite-difference Fortran algorithm, resulting in geometrical factor curves with trends that can be explained in terms of the boundary conditions of the probe and sampling volume. An examination of the geometrical factor curves provides additional insight that may be used to design, build and test future versions of the small drillhole minipermeameter probe.

Acknowledgements. The work described in this article was performed at Clemson University (Clemson, South Carolina) and supported by the U.S. Department of Energy (DOE), Fossil Energy Oil Technology Program, through the National Petroleum Technology Office under contract number DE-AC26-98BC15119. The views expressed in this article are those of the authors and do not necessarily reflect the views of the DOE. The authors are grateful to Lawrence C. Murdoch, Ronald W. Falta, Randall W. Fedors, and Budhi Sagar for contributions made at various stages of the project.

Notation

a internal tip seal radius and characteristic length of the conventional minipermeameter or the seal length ($D - L$) of the drillhole minipermeameter, L

A core plug cross-sectional area, L^2

B drillhole radius and characteristic length of the drillhole minipermeameter, L

B_D drillhole radius, dimensionless

D distance from rock face ($z = 0$) to proximal edge of angled injection boundary surface, L

D_D distance from rock face ($z_D = 0$) to proximal edge of angled injection boundary surface, dimensionless (D/B)

G_o geometrical factor, dimensionless

H distance from rock face ($z = 0$) to distal edge of seal, L

H_D distance from rock face ($z_D = 0$) to distal edge of seal, dimensionless (H/B)

i radial node index, matrix notation

j vertical node index, matrix notation

k_g apparent gas permeability, L^2

L core plug length, or distance from rock face ($z = 0$) to proximal edge of seal, L

L_D distance from rock face ($z_D = 0$) to proximal edge of seal, dimensionless (L/B)

$\dot{m}_o$ rate of gas mass injection, m/t

M_{wt} molar mass or molecular weight, m/mole

P_g gas pressure, mLt^{-2}/L^2

$P_{1,in}$ injection pressure, mLt^{-2}/L^2

$P_{0,out}$ atmospheric pressure, mLt^{-2}/L^2

q_1 volumetric flow rate, L^3/t

r radial coordinate direction, L

R gas constant

R_{max} distance to radial boundary, large enough to approximate infinity, L

R_{Dmax} distance to radial boundary, large enough to approximate infinity, dimensionless (R_{max}/B)

T absolute temperature, T

u_g Darcy "velocity" or Darcy flux, $L^3/L^2/t$

W depth of drillhole measured from rock face ($z = 0$), L

W_D depth of drillhole measured from rock face ($z_D = 0$), dimensionless (W/B)

z vertical coordinate direction, L

$\bar{z}$ average gas compressibility (or deviation) factor, dimensionless

Z_{max} distance to vertical boundary, large enough to approximate infinity, L

Z_{Dmax} distance to vertical boundary, large enough to approximate infinity, dimensionless (Z_{max}/B)

$\Delta\Phi$ $\Phi_1 - \Phi_0$

Φ gas pseudo-potential (a function of pressure-squared)

$\Phi_D(\Phi_1)$ dimensionless injection pseudo-potential

$\Phi_D(\Phi_0)$ dimensionless atmospheric pseudo-potential

μ_g gas viscosity, $m/L{\cdot}t$

π pi, radians

ρ_g gas density, m/L^3

φ dummy coordinate variable, L

θ angular coordinate direction, radians

ω successive-over-relaxation convergence amplification factor, dimensionless

$\bar{\nabla}$ gradient operator

$\bar{\nabla}\Phi_0$ pseudo-potential gradient at injection surface

References

Ali, M., *Small scale heterogeneities in permeability—a correlative study of permeability and corresponding pore morphologies using minipermeameter and petrographic analysis*, M.S. Thesis, New Mexico Institute of Mining and Technology, Socorro, New Mexico, 1993.

Allen, D., Probing for permeability: an introduction to measurements, *Tech. Review*, *36*(1), 6-20, 1988.

American Petroleum Institute, *Recommended Practice for Core Analysis Procedure*, API RP 40, American Petroleum Institute, Dallas, 1960.

American Petroleum Institute, *Recommended Practices for Core Analysis*, 2nd Edition, API RP 40, American Petroleum Institute, Dallas, 1998.

Aronson, E.C., *Modeling investigations on gas permeameters: spatial weighting functions and layered systems*, M.S. Special Project Report, New Mexico Institute of Mining and Technology, Socorro, New Mexico, 1999.

Bourke, L.T., Core permeability imaging: its relevance to conventional core characterization and potential application to wireline measurement, *Marine and Petroleum Geology, 10*, 318-324, 1993.

Castle, J.W., F.J. Molz, R.A. Bridges, C.L. Dinwiddie, C.J. Lorinovich, and S. Lu, *Quantitative methods for reservoir characterization and improved recovery: application to heavy oil sands*, Annual Report DOE-AC26-98BC15119, U.S. Department of Energy, Washington, D.C., 2000.

Chen, Z., *Mathematical basis for permeability and porosity measurements by minipermeameter*, M.S. Thesis, New Mexico Institute of Mining and Technology, Socorro, New Mexico, 1992.

Clelland, W., *Measurement and analysis of small scale permeability distributions in sandstones*, Ph.D. Dissertation, Heriot-Watt University, Edinburgh, Scotland, 1984.

Corbett, P.W.M. and J.L. Jensen, Variation of reservoir statistics according to sample spacing and measurement type for some intervals in the lower Brent Group, *The Log Analyst*. January-February, 22-41, 1992a.

Corbett, P.W.M. and J.L. Jensen, Estimating the mean permeability: how many measurements do you need? *First Break. 10*(3), 89-94, 1992b.

Dinwiddie, C.L., *A new small drillhole minipermeameter probe for in situ permeability measurement: design, theoretical analysis, operation, and performance characteristics*, Ph.D. Dissertation, Clemson University, Clemson, South Carolina, 2001.

Dinwiddie, C.L., F.J. Molz, III, L.C. Murdoch, and J.W. Castle, A new mini-permeameter probe and associated analytical techniques for measuring the *in situ* spatial distribution of permeability, *Eos Trans. AGU, 80*(46), American Geophysical Union Fall Meeting, San Francisco, CA, December 13-17, 1999.

Dubrule, O. and H.H. Haldorsen, Geostatistics for permeability estimation, in *Reservoir characterization*, edited by L.W. Lake and H.B. Carroll, Jr., pp. 223-247, Academic Press, Orlando, 1986.

Garrison, J.R., Jr., R.D. Hazlett, D.K. Babu, H. Laali, and L.D. Smallwood, Electronic flow rate-controlled probe permeametry: theory, instrumentation, accuracy, precision, limitations, and application, *In Situ, 20*(2), 161-198, 1996.

Gibbons, K., C. Halvorsen and E. Siring, Vertical and horizontal permeability variation within a sandstone reservoir based on minipermeameter measurements, *Marine and Petroleum Geology, 10*(4), 325-334, 1993.

Goggin, D.J., *Geologically-sensible modelling of the spatial distribution of permeability in eolian sandstone deposits: Page Sandstone (Jurassic), Northern Arizona*, Ph.D. Dissertation, University of Texas, Austin, Texas, 1988.

Goggin, D.J., Probe permeametry: is it worth the effort? *Marine and Petroleum Geology, 10*(4), 299-308, 1993.

Goggin, D.J., R.L. Thrasher, and L.W. Lake, A theoretical and experimental analysis of minipermeameter response, including gas slippage and high velocity flow effects. *In Situ, 12*(1&2), 79-116, 1988.

Halvorsen, C., Probe permeametry applied to a highly laminated sandstone reservoir. *Marine and Petroleum Geology, 10*(4), 347-351, 1993.

Halvorsen, C., and A. Hurst, Principles, practice and applications of laboratory minipermeametry, in *Advances in core evaluation, accuracy and precision in reserves estimation*, edited by P.F. Worthington, pp. 521-549, Gordon and Breach, Amsterdam, 1990.

Hassler, G., *Method and Apparatus for Permeability Measurements*. U.S. Patent Number 2,345,935, U.S. Patent Office, Washington D.C., 1944.

Hurst, A., Sedimentary flow units in hydrocarbon reservoirs: some shortcomings and a case for high-resolution permeability data, *Spec. Publ. int Ass. Sediment, 15*, 191-204, 1993.

Hurst, A., and K.J. Rosvoll, Permeability variations in sandstones and their relationship to sedimentary structures, in *Reservoir Characterization II*, edited by L.W. Lake, H.B. Carroll, Jr., and T.C. Wesson, pp. 166-196, Academic Press, San Diego, 1991.

Hurst, A., and D. Goggin. Probe permeametry: an overview and bibliography, *AAPG Bulletin, 79*(3), 463-473, 1995.

Hurst, A., C. Halvorsen, and E. Siring, A rationale for routine laboratory probe permeametry, *The Log Analyst, 36*(5), 10-20, 1995.

Jensen, J.L., A model for small-scale permeability measurement with applications to reservoir characterization, Proceedings of the *Seventh SPE/DOE Symposium on Enhanced Oil Recovery, SPE/DOE 20265*, pp. 891-900, Tulsa, April 22-25, 1990.

Jensen, J.L. and P.W.M. Corbett, A stochastic model for comparing probe permeameter and core plug measurements, in *Reservoir Characterization III*, edited by W. Linville, pp. 2-22, PennWell Books, Tulsa, 1992.

Jensen, J.L., C.A. Glasbey, and P.W.M. Corbett, On the interaction of geology, measurement, and statistical analysis of small-scale permeability measurements, *Terra Nova, 6*, 397-403, 1994.

Jones, S.C., The profile permeameter: a new, fast, accurate minipermeameter, Proceedings of the *67th Annual Technical Conference of the SPE, SPE 24757*, pp. 973-983, Washington D.C., October 4-7, 1992.

Kara, B., E. Kasap, and R.W. Tillman, Quantitative description of muddy sandstone: geostatistical parameters, automated facies generations, and measurement methodologies, Proceedings of the *68th Annual Technical Conference and Exhibition of the Society of Petroleum Engineers, SPE 26488*, pp. 741-756, Houston, October 3-6, 1993.

Norris, R.J. and J.J.M. Lewis, The geological modeling of effective permeability in complex heterolithic facies, Proceedings of the *66th Annual Technical Conference and Exhibition of the Society of Petroleum Engineers, SPE 22692*, pp. 359-374, Dallas, October 6-9, 1991.

Pickup, G.E., P.S. Ringrose, P.W.M. Corbett, J.L. Jensen, and K.S. Sorbie, Geology, geometry and effective flow, *Petroleum Geoscience, 1*, 37-42, 1995.

Robertson, G.M. and C.A. McPhee, High-resolution probe permeability: an aid to reservoir description, Proceedings of the First Society of Core Analysis Symposium in *Advances in core evaluation, accuracy and precision in reserves estimation*, London, May 21-23, 1990, edited by P.F. Worthington, pp. 495-520, Gordon and Breach, Amsterdam, 1990.

Sharp, J.M., L. Fu, P. Cortez, and E. Wheeler, An electronic minipermeameter for use in the field and laboratory, *Ground Water*, *32*(1), 41-46, 1994.

Suboor, M.A., and J.P. Heller, Minipermeameter characteristics critical to its use, *In Situ*, *19*(3), 225-248, 1995.

Sutherland, W.J., C. Halvorsen, A. Hurst, C.A. McPhee, G. Robertson, P.R. Whattler, and P.F. Worthington, Recommended practice for probe permeametry, *Marine and Petroleum Geology*, *10*(4), 309-317, 1993.

Tidwell, V.C. and J.L. Wilson, Laboratory method for investigating permeability upscaling, *Water Resour. Res.*, *33*(7), 1607-1616, 1997.

Weber, K.J., Influence of common sedimentary structures on fluid flow in reservoir models, *Journal of Petroleum Technology*, *34*(3), 665-672, 1982.

Weber, K.J., How heterogeneity affects oil recovery, in *Reservoir Characterization*, edited by L.W. Lake and H.B. Carrol, Jr., Academic Press, Orlando, 487-544, 1986.

Young, G.R., *Determining permeability anisotropy from a core plug using a minipermeameter*, M.S.E. Thesis, The University of Texas, Austin, Texas, 1989.

Zheng, S., P.W.M. Corbett, A. Ryseth, and G. Stewart, Uncertainty in well test and core permeability analysis: a case study in fluvial channel reservoirs, northern North Sea, Norway, *AAPG Bulletin*. *84*(12), 1929-1954, 2000.

J.W. Castle, Clemson University, Department of Geological Sciences, Brackett Hall, P.O. Box 340976, Clemson, SC 29632-0976. (jcastle@clemson.edu)

[1]C.L. Dinwiddie, Southwest Research Institute, Center for Nuclear Waste Regulatory Analyses, 6220 Culebra Road, San Antonio, TX 78238-5166. (cdinwiddie@swri.org)

F.J. Molz, III, Clemson University, Department of Environmental Engineering & Science, 342 Computer Court, Anderson, SC 29625. (fredi@clemson.edu)

(Received;)

[1]Formerly at Clemson University, Department of Environmental Engineering & Science.

Figure Captions

Figure 1. The new small drillhole minipermeameter probe. Rotating the torque wheel clockwise moves the sliding sleeve toward the distal end of the probe, causing the seal to compress and radially expand.

Figure 2. Model geometry for the small drillhole minipermeameter probe. The drill hole is cylindrical with a tapered end reflecting the shape of the drill bit; the rubber seal is shown in black.

Figure 3. a) Mesh system for the entire flow domain of the field probe model; b) expanded portion of mesh near end of drilled hole.

Figure 4. Methodology for determination of minimum far-field boundaries. Examination of geometrical factor sensitivity to edge effects indicates that R_{Dmax} and Z_{Dmax} should be set to roughly 100 dimensionless length units in order to approximate an infinite half-space for the geometry of the laboratory and field-tested drillhole probe system.

Figure 5. Numerical solution for the dimensionless pseudo-potential field in the vicinity of the small drillhole minipermeameter field probe. Contours are lines of constant dimensionless pseudo-potential, and arrows indicate the orthogonal streamtraces expected in an isotropic and homogeneous medium.

Figure 6. Numerical solution for the dimensionless pseudo-potential field of the small drillhole minipermeameter probe when in a drill hole of the shallowest possible depth (where the dimensionless seal length, radius, and vertical headspace are equivalent to those used during fieldwork). Contours are lines of constant dimensionless pseudo-potential, and arrows indicate the orthogonal streamtraces expected in an isotropic and homogeneous medium.

Figure 7. Geometrical factor sensitivity to increasing dimensionless drillhole depth, W_D, when the dimensionless expanded seal length, a_D, headspace, H_D, and drillhole radius remain constant.

Figure 8. Numerical solution for the dimensionless pseudo-potential field of the small drillhole minipermeameter probe when subject to a very long seal or packer (while the dimensionless vertical headspace, drillhole depth, and radius are equivalent to those used during fieldwork). Contours are lines of constant dimensionless pseudo-potential, and arrows indicate the orthogonal streamtraces expected in an isotropic and homogeneous medium.

Figure 9. Geometrical factor sensitivity to both increasing dimensionless seal length, $a_D = H_D - L_D$, and decreasing dimensionless distance to the seal, L_D, when the vertical headspace, H_D, is held constant.

Figure Captions (continued)

Figure 10. Numerical solution for the dimensionless pseudo-potential field of the small drillhole minipermeameter probe flow system with an increased head-space or injection area (i.e., the probe isn't fully inserted into the drill hole), while keeping the dimensionless seal length, radius, and drillhole depth equivalent to those used during fieldwork. Contours are lines of constant dimensionless pseudo-potential, and arrows indicate the orthogonal streamtraces expected in an isotropic and homogeneous medium.

Figure 11. The geometrical factor exhibits a linear dependence on the dimensionless headspace, given here as H_D, when the dimensionless drillhole depth, W_D, and seal length, $a_D = H_D - L_D$, are held constant.

Figure 12. Geometrical factor sensitivity again exhibits a linear dependence on the area available for injection. In this case the geometrical factor is a linear function of the drillhole radius of a flattened drillhole (no conical drill bit shape at the distal end; the seal length, $a = H - L$, was defined to be the characteristic length for this case, *not* the drillhole radius, B).

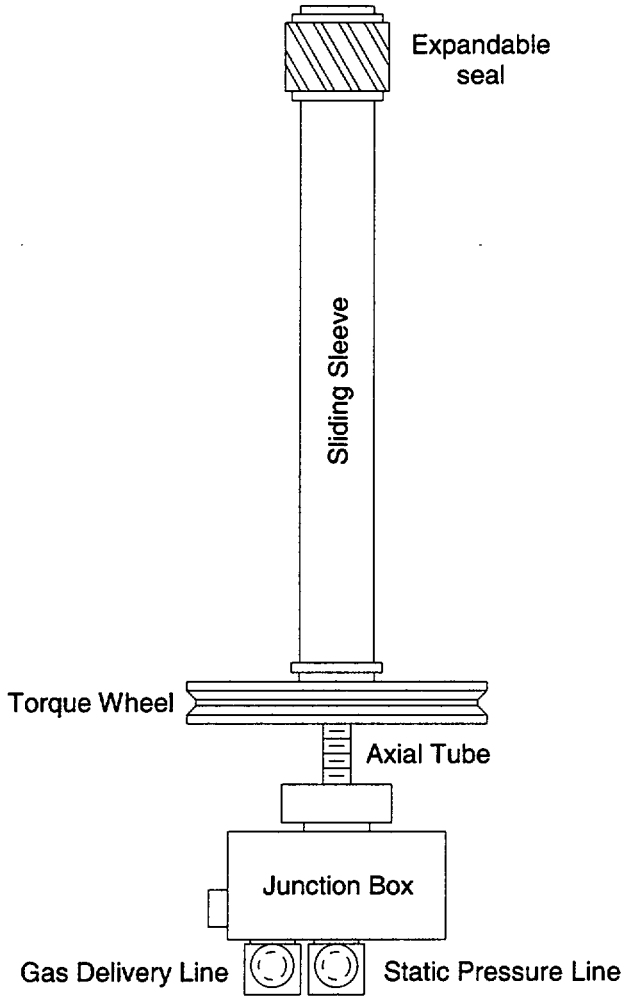

Figure 1. The new small drillhole minipermeameter probe. Rotating the torque wheel clockwise moves the sliding sleeve toward the distal end of the probe, causing the seal to compress and radially expand.

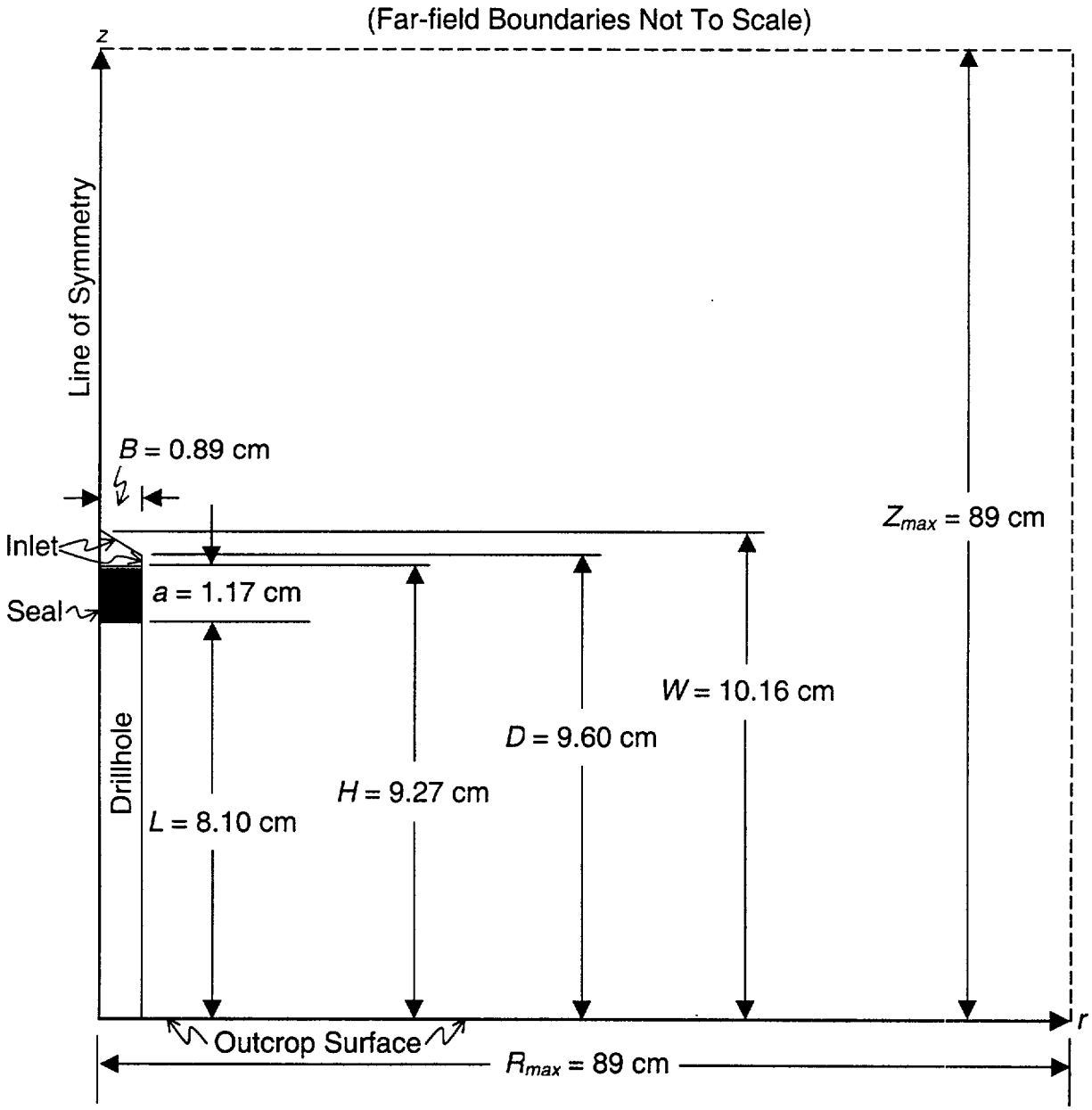

Figure 2. Model geometry for the small drillhole minipermeameter probe. The drill hole is cylindrical with a tapered end reflecting the shape of the drill bit; the rubber seal is shown in black.

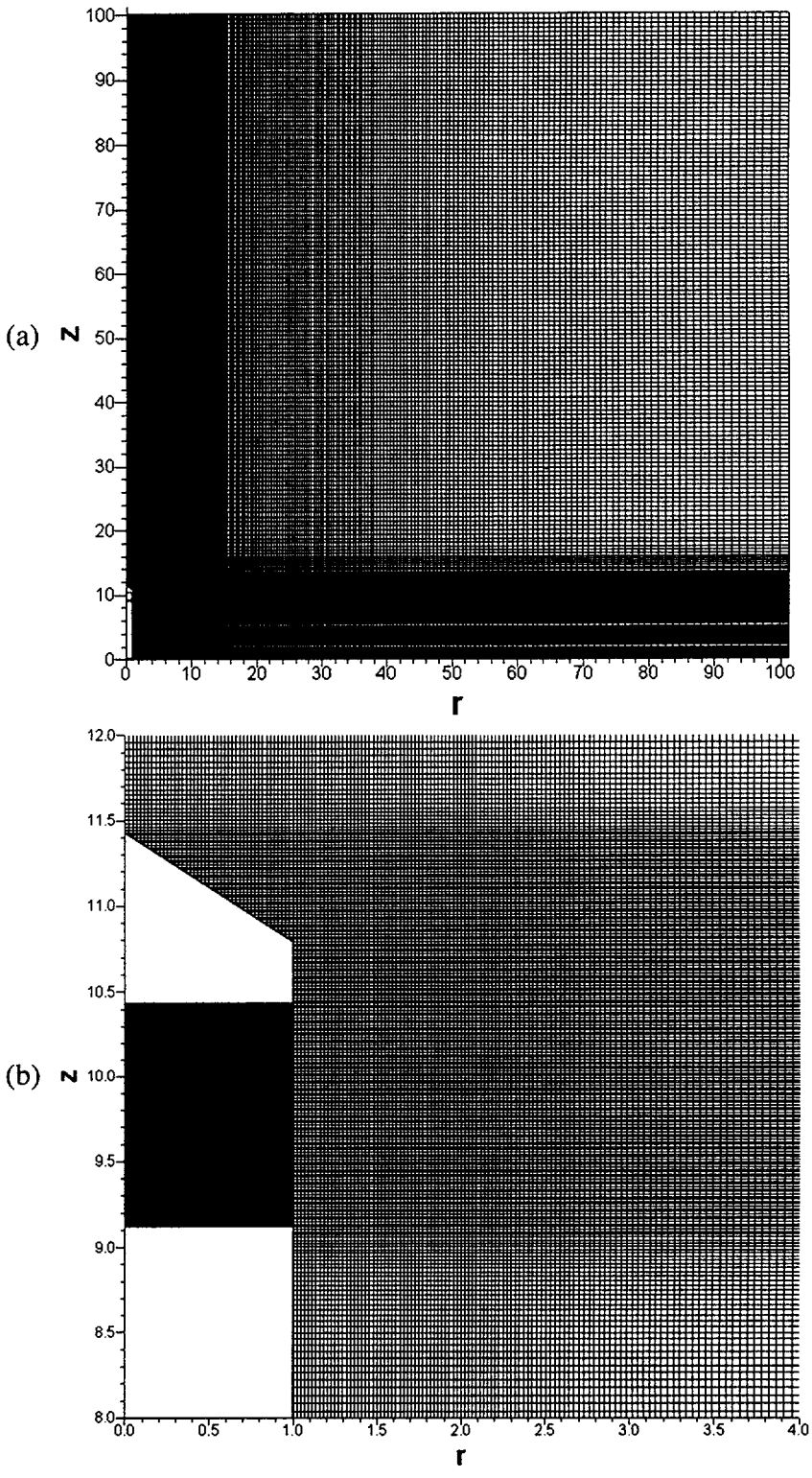

Figure 3. a) Mesh system for the entire flow domain of the field probe model; b) expanded portion of mesh near end of drilled hole.

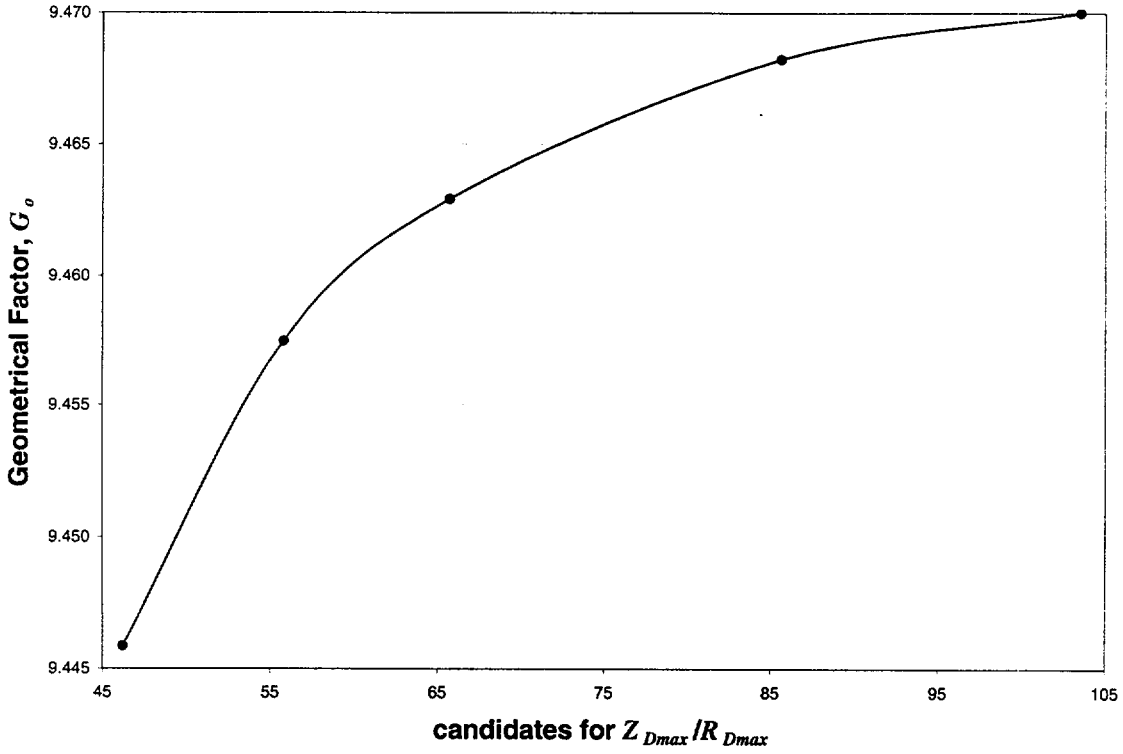

Figure 4. Methodology for determination of minimum far-field boundaries. Examination of geometrical factor sensitivity to edge effects indicates that R_{Dmax} and Z_{Dmax} should be set to roughly 100 dimensionless length units in order to approximate an infinite half-space for the geometry of the laboratory and field-tested drillhole probe system.

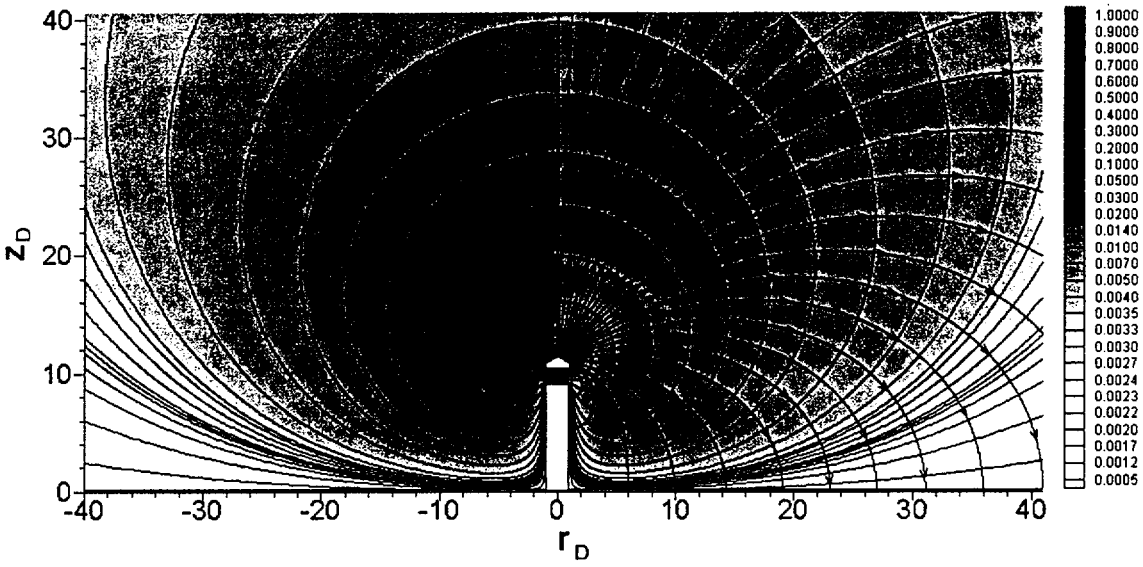

Figure 5. Numerical solution for the dimensionless pseudo-potential field in the vicinity of the small drillhole minipermeameter field probe. Contours are lines of constant dimensionless pseudo-potential, and arrows indicate the orthogonal streamtraces expected in an isotropic and homogeneous medium.

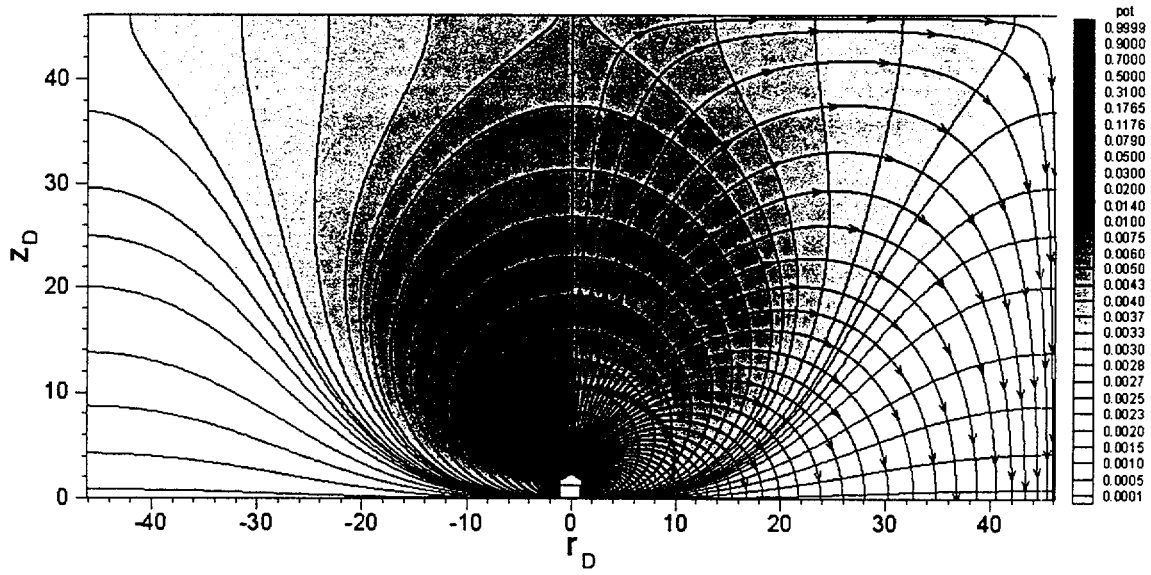

Figure 6. Numerical solution for the dimensionless pseudo-potential field of the small drillhole minipermeameter probe when in a drill hole of the shallowest possible depth (where the dimensionless seal length, radius, and vertical headspace are equivalent to those used during fieldwork). Contours are lines of constant dimensionless pseudo-potential, and arrows indicate the orthogonal streamtraces expected in an isotropic and homogeneous medium.

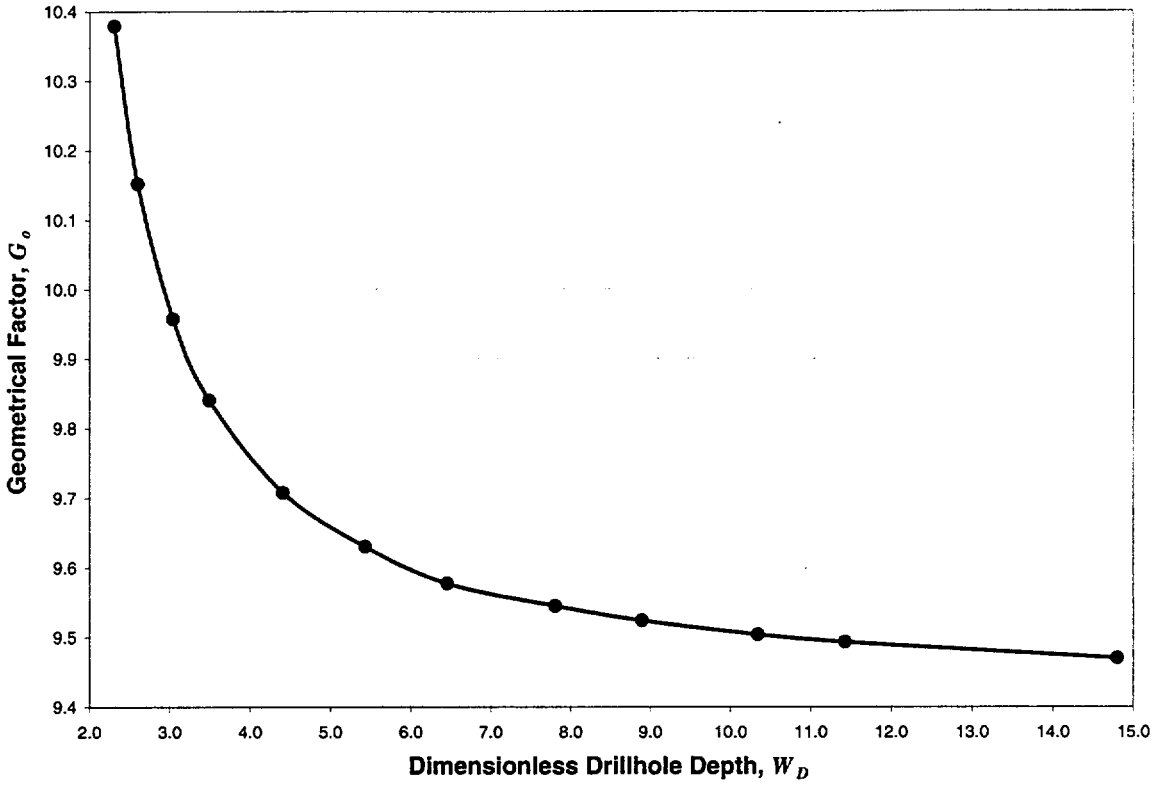

Figure 7. Geometrical factor sensitivity to increasing dimensionless drillhole depth, W_D, when the dimensionless expanded seal length, a_D, headspace, H_D, and drillhole radius remain constant.

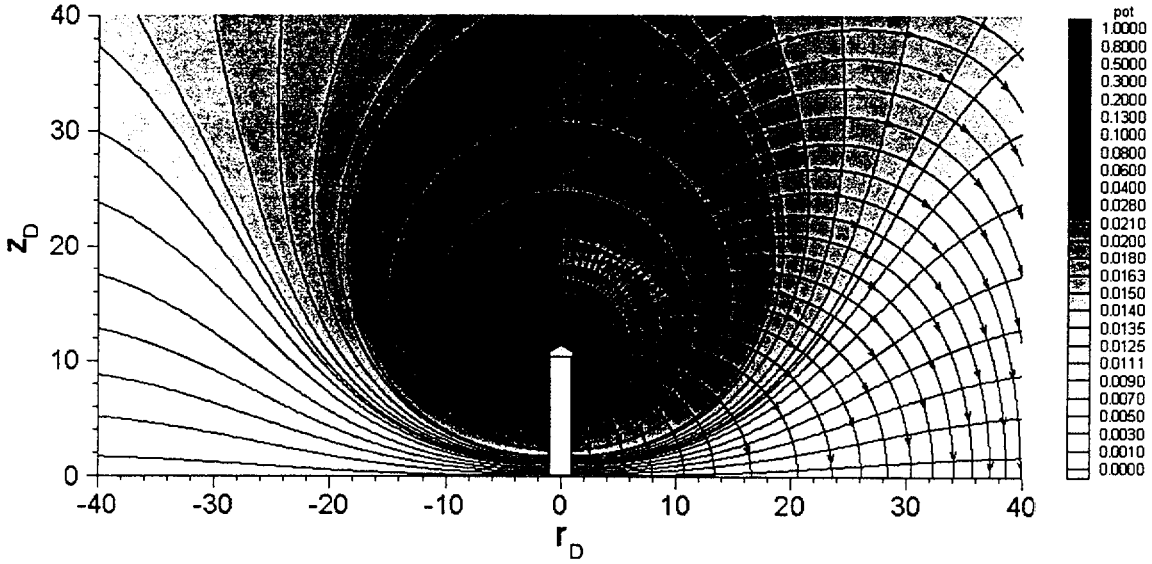

Figure 8. Numerical solution for the dimensionless pseudo-potential field of the small drillhole minipermeameter probe when subject to a very long seal or packer (while the dimensionless vertical headspace, drillhole depth, and radius are equivalent to those used during fieldwork). Contours are lines of constant dimensionless pseudo-potential, and arrows indicate the orthogonal streamtraces expected in an isotropic and homogeneous medium.

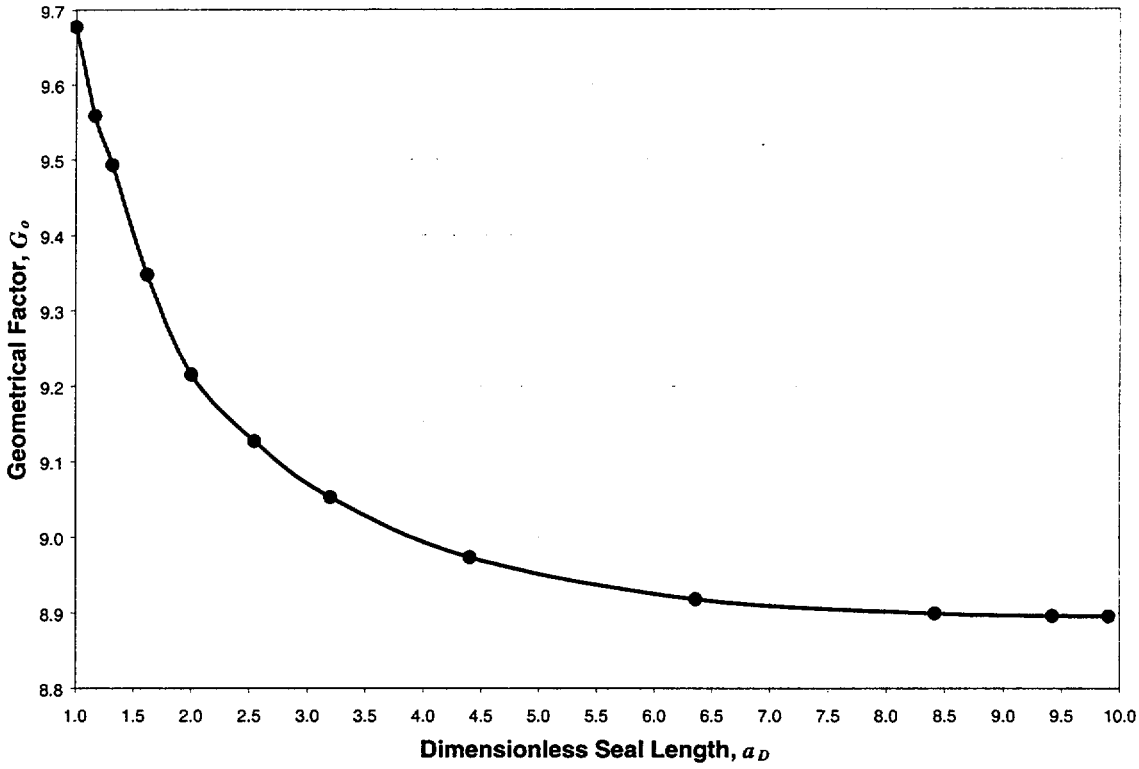

Figure 9. Geometrical factor sensitivity to both increasing dimensionless seal length, $a_D = H_D - L_D$, and decreasing dimensionless distance to the seal, L_D, when the vertical headspace, H_D, is held constant.

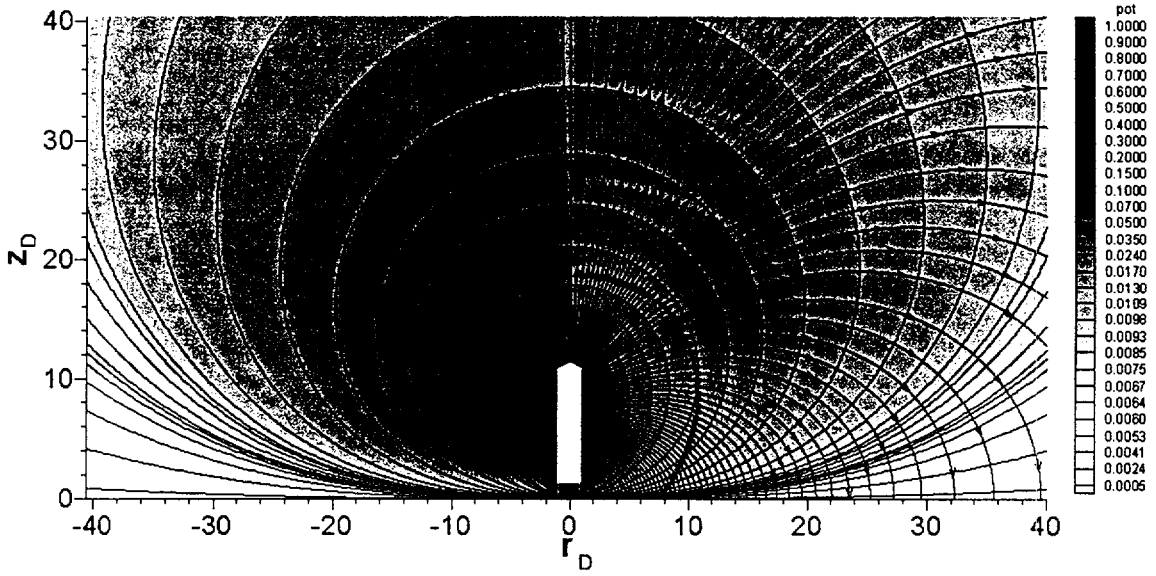

Figure 10. Numerical solution for the dimensionless pseudo-potential field of the small drillhole minipermeameter probe flow system with an increased head-space or injection area (i.e., the probe isn't fully inserted into the drill hole), while keeping the dimensionless seal length, radius, and drillhole depth equivalent to those used during fieldwork. Contours are lines of constant dimensionless pseudo-potential, and arrows indicate the orthogonal streamtraces expected in an isotropic and homogeneous medium.

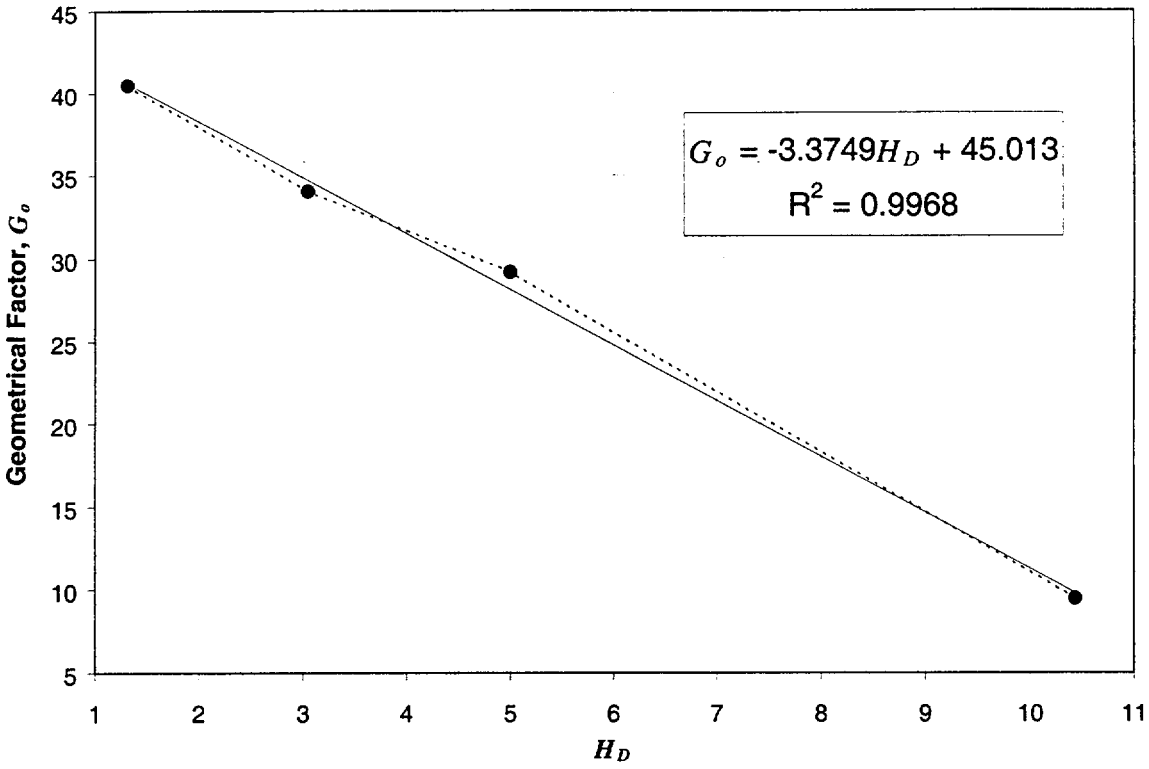

Figure 11. The geometrical factor exhibits a linear dependence on the dimensionless headspace, given here as H_D, when the dimensionless drillhole depth, W_D, and seal length, $a_D = H_D - L_D$, are held constant.

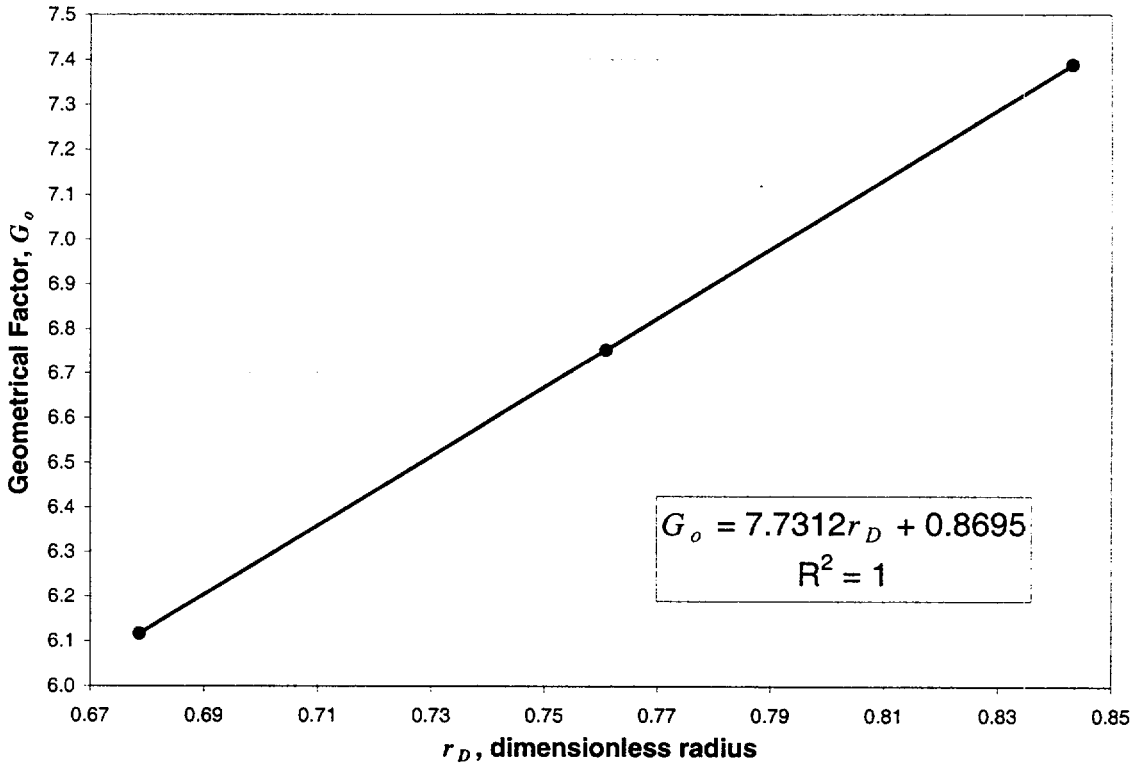

Figure 12. Geometrical factor sensitivity again exhibits a linear dependence on the area available for injection. In this case the geometrical factor is a linear function of the drillhole radius of a flattened drillhole (no conical drill bit shape at the distal end; the seal length, $a = H - L$, was defined to be the characteristic length for this case, *not* the drillhole radius, B).